In vivo RyR1 reduction in muscle triggers a core-like myopathy

Laurent Pelletier[1†], Anne Petiot[1†], Julie Brocard[1], Benoit Giannesini[2†], Diane Giovannini[1†], Colline Sanchez[3], Lauriane Travard[1], Mathilde Chivet[1], Mathilde Beaufils[1], Candice Kutchukian[3], David Bendahan[2], Daniel Metzger[4], Clara Franzini Armstrong[5], Norma B. Romero[6], John Rendu[1], Vincent Jacquemond[3], Julien Fauré[1] and Isabelle Marty[1*]

Abstract

Mutations in the *RYR1* gene, encoding the skeletal muscle calcium channel RyR1, lead to congenital myopathies, through expression of a channel with abnormal permeability and/or in reduced amount, but the direct functional whole organism consequences of exclusive reduction in RyR1 amount have never been studied. We have developed and characterized a mouse model with inducible muscle specific *RYR1* deletion. Tamoxifen-induced recombination in the *RYR1* gene at adult age resulted in a progressive reduction in the protein amount reaching a stable level of 50% of the initial amount, and was associated with a progressive muscle weakness and atrophy. Measurement of calcium fluxes in isolated muscle fibers demonstrated a reduction in the amplitude of RyR1-related calcium release mirroring the reduction in the protein amount. Alterations in the muscle structure were observed, with fibers atrophy, abnormal mitochondria distribution and membrane remodeling. An increase in the expression level of many proteins was observed, as well as an inhibition of the autophagy process. This model demonstrates that RyR1 reduction is sufficient to recapitulate most features of Central Core Disease, and accordingly similar alterations were observed in muscle biopsies from Dusty Core Disease patients (a subtype of Central Core Disease), pointing to common pathophysiological mechanisms related to RyR1 reduction.

Keywords: Ryanodine receptor, Calcium, Skeletal muscle, Excitation–contraction coupling, Congenital myopathies, Central core disease, Dusty core disease, Mouse model

Introduction

One key step for skeletal muscle contraction is the intracellular calcium release performed by the sarcoplasmic reticulum calcium channel ryanodine receptor (RyR1) during the excitation–contraction coupling process. RyR1 is the core of the Calcium Release Complex (CRC), anchored both in the sarcoplasmic reticulum (SR) membrane and the T-tubule membrane, in a specific region of the muscle called the triad where these two membranes are in close apposition. Additional proteins are associated with RyR1 to form the CRC, including the voltage-activated plasma membrane calcium channel dihydropyridine receptor (DHPR) [1], and regulatory proteins like the sarcoplasmic reticulum calcium binding protein calsequestrin (CSQ), or the sarcoplasmic reticulum membrane proteins triadin and junctin [2]. Numerous mutations in the *RYR1* gene encoding the ryanodine receptor result in genetic diseases among which two core myopathies:

*Correspondence: isabelle.marty@univ-grenoble-alpes.fr
†Laurent Pelletier and Anne Petiot have contributed equally.
†Benoit Giannesini, Diane Giovannini, and Colline Sanchez have contributed equally.
[1] INSERM, GIN-U1216, CHU Grenoble Alpes, Grenoble Institut Neurosciences, University Grenoble Alpes, Bat EJ Safra, Chemin Fortuné Ferrini, La Tronche, Grenoble, France
Full list of author information is available at the end of the article

Central Core Disease (CCD, OMIM#117000) and Multiminicore disease (MmD, OMIM#255320). The impact of *RYR1* mutations are either an alteration of the RyR1 calcium channel function (gain- or loss-of-function), a modification of the RyR1-DHPR coupling, or the reduction in the amount of RyR1 protein. In all cases, the consequence is a reduction in the amplitude of calcium release upon stimulation, resulting in muscle weakness [3–8]. To explore the various pathophysiology mechanisms associated with *RYR1* mutations, different mouse models have been created. They mostly reproduce amino acid substitutions in the RyR1 protein associated with mutations identified in patients in dominant (Y522S, I4898T) [9, 10] or recessive pathologies (T4706M + del; Q1970fsX16 + A4329D) [11–13]. These models have been useful to better understand some aspects of RyR1 physiology and to confirm the pathogenicity of patients' mutations, but reveal mechanisms that are specific to individual or to a combination of RyR1 mutations. The recently developed recessive models combined an hypomorphic allele with a point mutation [11, 12], and therefore, on a mechanistic point of view, presented with both important reduction in RyR1 amount and expression of a mutant channel with altered calcium permeability.

In the present work we focused on the pathophysiology of the exclusive reduction in RyR1 protein expression in muscle, as this situation is frequently observed in patients affected with recessive congenital myopathy. To dissect the mechanisms related to a reduction in RyR1 amount we have developed and characterized a mouse model with a conditional and inducible *RYR1* knock out. In mice, the full deletion of the *RYR1* gene is lethal at birth [14], and heterozygous deletion of a single *RYR1* allele results only in a modest 15% reduction in RyR1 protein, with no functional consequences [15]. In order to obtain a model with reduced amount of RyR1 specifically in skeletal muscles, we have developed a new mouse line RyR1$^{Flox/Flox}$::HSA-Cre-ER^{T2} in which a decreased *RYR1* expression is induced by tamoxifen injection. We show that few weeks after induction, the amount of RyR1 protein reached 50% of initial level, and the mice developed a progressive myopathy, which recapitulates the main features observed in patients affected with Dusty Core Disease and with a similar RyR1 reduction [16]. Dusty Core Disease has been recently described as a subgroup of recessive Central Core Disease characterized by severe phenotype, early onset, low RyR1 expression, and histological lesions so-called dusty cores which differ from the classical central cores (well delimited region depleted in mitochondrial enzymatic activity) by the presence of regions within the same fiber of blended increase/decrease enzymatic activity (dusty cores) [16]. This model which presents the same molecular and structural modifications as patients could therefore be a valuable tool for further pathophysiological mechanisms dissection and for therapeutic development.

Materials and methods
Engineering of the mouse model
The RyR1-flox mouse line has been established at the MCI/ICS (Mouse Clinical Institute, Illkirch, France; http://www-mci.u-strasbg.fr). LoxP sites were introduced by homologous recombination in ES cells on both sides of exons 9–11 of the *RYR1* gene. The HSA-Cre-ER^{T2} mouse line, in which the expression of the tamoxifen dependent Cre-ER^{T2} recombinase is under the control of the human skeletal muscle α-actin gene, has been described previously [17]. In this transgenic line Cre-ER^{T2} is selectively expressed in skeletal muscles fibers and activated upon tamoxifen injection, and Cre-ER^{T2}-mediated alteration of LoxP (floxed) target genes is skeletal muscle-specific and strictly tamoxifen dependent. The two mouse lines were on a a C57BL/6 J background and intercrossed to create the RyR1$^{flox/flox}$::HSA-Cre-ER^{T2} mouse line. Mice were given ad libitum access to food and water, food pellets were provided directly in the cage to ensure a correct feeding.

Antibodies and reagents
Rabbit polyclonal antibody against RyR1, Trisk 95 and Trisk 51 and guinea pig anti-RyR1 C-terminal peptide have been previously described [1, 18, 19], as well as antibodies against SERCA (kindly provided by Moutin [20]), and antibody against the FoF1-ATPase (kindly provided by Lunardi [21]). Antibody against the alpha subunit of DHPR was from Abcam (ref ab2862), antibody against STIM1 from Merck Millipore (ref AB9870), antibody against CSQ1 was ThermoFisher (ref MA3-913), antibody against CLIMP63 from Bethyl (Rabbit anti-CKAP4 antibody, ref A302-257A), antibody against Orai1 from Alomone labs (ref ACC-062), antibody against desmin from Dako (ref M0724), polyclonal antibody against alpha-actinin from Sigma Aldrich (ref SAB4503474), antibody against p62 from Abnova (SQSTM1 monoclonal antibody clone 2C11 ref H00008878-M01), antibody against LC3A/B from Cell Signaling Technology (ref 4108), as well as antibody against mTOR and P-mTOR (ref 2972 and 2971 respectively), antibody against S6 and P-S6 (ref 2217 and 2215 respectively), rabbit mAb against GAPDH (14C10, ref 2128S). Secondary antibodies used for Western blot were labelled with HRP (Jackson Immuno Research), and the antibodies used for immunofluorescent staining were labelled with Alexa fluor 488, Cy-3 or Cy-5 (Jackson Immuno Research). Tamoxifen was from Sigma Aldrich.

Reverse transcription-quantitative PCR (RT-qPCR)

Target gene transcript expression was measured by quantitative real-time polymerase chain reaction (RT-qPCR). Total RNA was isolated from muscle tissue using NucleoSpin RNA Set for NucleoZOL (Macherey–Nagel). RNA was quantified using a NanoDrop 1000 spectrophotometer (Thermo Scientific, Waltham, MA). RNA was reverse transcribed using iScript Reverse Transcription Supermix for RT-PCR (Bio-Rad Laboratories, Hercules, CA). Then RT-qPCR was conducted using SsoAdvanced™ Universal SYBR® Green Supermix (Bio-Rad Laboratories), and 1 µl cDNA was used to detect the transcript of interest. All reactions were run in duplicate. RT-qPCR reactions were run on an CFX96 Touch™ Real-Time PCR Detection System (Bio-Rad). The primer sequences were designed using Vector NTI software (Thermo-Fischer). The amplification steps were the following: 50 °C–2 min; 95 °C–10 min; 40 cycles composed of 95 °C–15 s, 60 °C–30 s, 72 °C–30 s; 72 °C–10 min. A threefold RNA dilution series was used to determine efficiency of each qPCR assay. Efficiency of all qPCRs was between 95 and 105%. Amplification data were analyzed with CFX manager software (Bio-Rad). Expression was normalized to three endogenous controls (beta-actin, HPRT and GAPDH) using the $\Delta\Delta C_t$ method. The primers (forward and reverse) used for PCR amplification are listed in Table 1.

Western blot analysis and quantification

Western blot analysis was performed on muscle homogenates as previously described [16]. Briefly, after electrophoretic separation on a 4–20% gradient acrylamide gel (Stain-free precast gel, Biorad, France) and electrotransfer to Immobilon P (Biorad, France), the membrane was incubated with primary antibodies and then HRP-labelled secondary antibodies (Jackson ImmunoResearch Laboratories). Signal quantification was performed using a ChemiDoc Touch apparatus (Biorad, France) and the Image Lab software (Biorad). The amount of the chosen protein in each sample was corrected for differences in loading using either the amount of myosin, GAPDH or the total amount of proteins using the stain free system from Biorad, and

normalized to the amount of the same protein present in the control, set to 100% as described previously [15]. Ten human controls (muscle biopsy from individuals non-affected by neuromuscular disease) of different age have been used, from 3.5 to 64 years. For each sample (mouse and human), 2–3 Western blots have been performed, and the value for each sample corresponds to the mean ± SEM of the different Western blots.

Grip test

The animals were trained 3 times on 3 different days over the week before tamoxifen injection, and they were subsequently tested once a week until muscle collection. The animals were positioned on a cross-wired surface where they could hold on with all four paws. The grid was then turned upside down, and the time during which each animal was able to stay on wires before falling was recorded, up to a maximum of 300 s (5 min). Three falls were allowed.

Noninvasive investigation of gastrocnemius muscle function and bioenergetics

Gastrocnemius muscle anatomy and mechanical performance were investigated noninvasively and longitudinally using MR measurements in 8 controls and 6 RyR1-Rec littermates every month at D30, D60 and D90 after tamoxifen injection. Additionally, muscle energy metabolism was assessed at D60 simultaneously to mechanical performance acquisition. Anesthetized mice were placed into a home-built cradle allowing the MR investigation of the left gastrocnemius muscle function and bioenergetics in a preclinical 47/30 Biospec Avance MR scanner (Bruker, Karlsruhe, Germany) as described previously [22, 23]. Ten axial anatomic images (1-mm thickness; 0.5-mm spaced; 0.117×0.117 mm^2 spatial resolution) covering the region from the knee to the ankle were acquired at rest. Mechanical performance was recorded using a dedicated ergometer during a fatiguing bout of exercise electrically induced by square-wave pulses (1 ms duration) with transcutaneous surface electrodes and consisting in 6 min of maximal isometric contractions repeated at a frequency of 1.7 Hz. At D60, concentrations of high-energy phosphorylated compounds and pH were

Table 1 Primers for RT-qPCR

Target gene	Forward	Reverse
ACTB	CTAAGGCCAACCGTGAAAAG	ACCAGAGGCATACAGGGACA
GAPDH	CGTGCCGCCTGGAGAAAC	TGGGAGTTGCTGTTGAAGTCG
HPRT	CCTAATCATTATGCCGAGGATTTGG	CCCATCTCCTTCATGACATCTCGAG
RYR-1	GGTCTGATTATTGATGCTTTTGGGG	TGGTCTCCATGTCTTCCTTCACTTG

continuously measured using dynamic ^{31}P-MR spectroscopy during rest (6 min), exercise (6 min) and post-exercise recovery period (16 min). MR data were processed using custom-written analysis programs developed on the IDL software (Research System, Boulder, CO).

Histological staining
Ten μm thick cryostat *Tibialis anterior* (TA) sections (Cryostar Nx70, Thermo Scientific) were stained with haematoxylin and eosin (HE), modified Gomori trichrome (GT) and reduced nicotinamide adenine dinucleotide dehydrogenase-tetrazolium reductase (NADH-TR), and observed using a Leica ICC 50 microscope.

Electron microscopy
EDL muscles of RyR1-Rec male mice 75 days after tamoxifen injection (4.5 months old) were excised, cut into small pieces and prepared as described before [22]. The sections were observed with a Jeol JEM 1200EX II at 60 kV.

Immunofluorescent labelling
EDL muscles were collected from CTRL and RyR1-Rec littermates 75 days after tamoxifen injection. After 15 min fixation at RT in 4% PFA diluted in PBS, the fibers were manually dissociated using needles to comb the fibers, and the triple labelling was performed as described previously [22] using primary antibodies developed in guinea pig, rabbit or mouse, and anti-species secondary antibodies labelled with either Alexa fluor 488, Cy 3 or Cy 5. The images are representative of at least 3 animals in each group.

Electrophysiology and confocal fluorescence imaging in isolated muscle fibers
Single fibers were isolated from the *flexor digitorum brevis* (FDB) and *interosseus* muscles following previously described procedures [24–26]. In brief, muscles were digested by incubation with collagenase followed by trituration to produce dissociated fibers. All experiments were performed at room temperature (20–22 °C). Membrane depolarizing steps of 0.5 s duration were applied from a holding potential of -80 mV to the single fibers partly insulated with silicone grease, and the resulting voltage-activated Ca^{2+} transients was measured using the dye rhod-2 introduced into the fiber by the patch pipette. The detailed electrophysiological procedures are described in Additional file 1: Supplementary method.

Statistics
The statistical analysis has been done with GraphPad Prism 6.0 software. The number of samples and the name of the parametric test applied are indicated in each figure legend. Results are considered as significant when $p < 0.05$, the exact value for p being indicated in the text or figure legends, and significant results are labeled * on the graphs whatever the exact p value. All data are shown as mean $\pm$ SEM.

Results

Generation of the RyR1$^{Flox/Flox}$::HSA-Cre-ER^{T2} mouse model
A mouse line with loxP sites inserted on both side of exons 9–11 of the *RYR1* gene (so called RyR1$^{Flox/Flox}$) was mated with the mouse line HSA-Cre-ER^{T2} expressing the tamoxifen dependent Cre-ER^{T2} recombinase under the control of the human skeletal muscle α-actin gene [17], to create RyR1$^{Flox/Flox}$::HSA-Cre-ER^{T2}. Tamoxifen injection induces activation of the Cre-ER^{T2} recombinase selectively in skeletal muscle, which results in the deletion of exons 9–11 and disruption of the *RYR1* gene in skeletal muscle with a strict tamoxifen dependence (Fig. 1a). At birth, RyR1$^{Flox/Flox}$::HSA-Cre-ER^{T2} mice were normal, and at 2 months of age, once young adults, the recombination was induced by tamoxifen injection (from this time point, the recombined animals were called RyR1-Rec). Molecular and physiological consequences were further studied as a function of time, up to 105 days after induction of recombination (Fig. 1b). Control animals (CTRL) are littermates RyR1$^{Flox/Flox}$ (without the HSA-Cre-ER^{T2} transgene) injected with tamoxifen. The overall phenotype of the recombined mice at 75 days is characterized by a kyphosis associated with an abnormal mobility of the hind limbs and a waddling walking. The animals are still able to stand on their rear feet to feed, but food pellets had been systematically given directly in the cage as the disease progressed. At 105 days, the animals are still mobile in their cages and no increased death rate observed compared to CTRL. Both males and females were affected. The relative amount of RyR1 at the mRNA level was analyzed in quadriceps muscle every 15 days after recombination using RT-q-PCR in CTRL and in RyR1-Rec animals (Fig. 1c). A rapid drop in RyR1 mRNA was observed, with a low and stable level of 21% $\pm$ 4% of the initial value reached as soon as 3 days after tamoxifen injection. A reduction was observed in all of the tested muscles 75 days after recombination induction (*Quadriceps*, *tibialis anterior, EDL, soleus*, Additional file 1: Fig. S1A). The amount of RyR1 protein was further analyzed, using quantitative Western blot in quadriceps muscle homogenates (Fig. 1d, e). This amount was progressively reduced and reached about 50% of initial value after 105 days. No further reduction in RyR1 protein was observed on longer times (data not shown). The amount of RyR1 protein was quantified in different muscle homogenates 75 days after recombination. A reduction
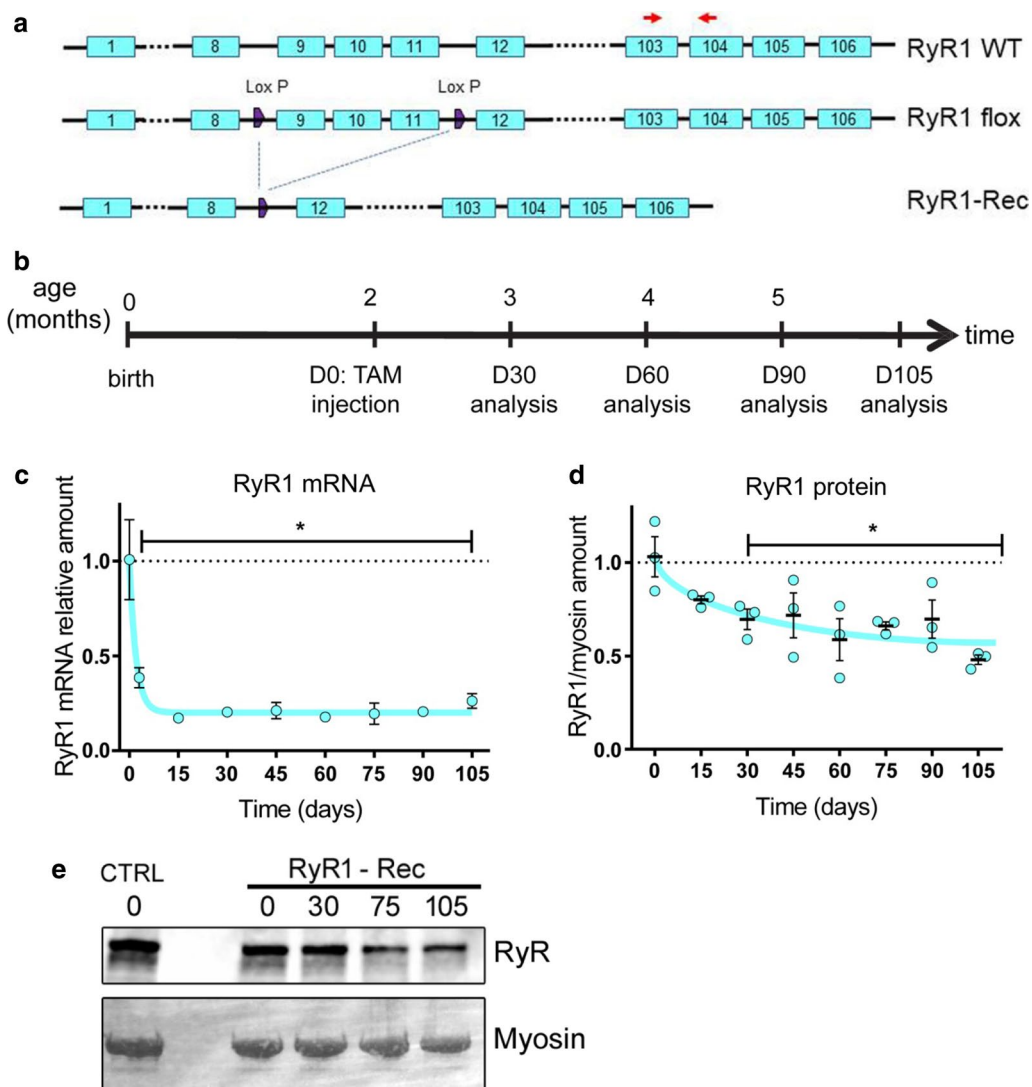
Fig. 1 RyR1 mRNA and protein decrease after tamoxifen injection in the RyR1^Flox/Flox^::HSA-Cre-ER^T2^ mouse model. **a** LoxP sites were inserted on both sides of exons 9-11 in the RyR1 WT allele to create the RyR1-flox allele. After recombination, the RyR1-Rec allele is deleted with exons 9-11. The primers used for the RT-q-PCR amplification of RyR1 transcript of panel care represented by the red arrows respectively in exon 103 and 104. **b** The animals were injected with tamoxifen to induce the recombination at 2 months of age (D0), and were analyzed at variable times thereafter. **c** The relative amount of mRNA compared to beta-actin, HPRT and GAPDH as reference genes were evaluated using RT-q-PCR in quadriceps muscles of n = 3–6 different mice at each time point, and is presented as mean ± SEM for each time. The amount in CTRL littermate was set to 1. The quantification was performed using the $\Delta\Delta C_t$ method. Statistical analysis: One way ANOVA with Holm–Sidack's test for multiple comparisons. **d** The relative amount of RyR1 compared to myosin heavy chain was evaluated using quantitative Western blot in quadriceps homogenates of n = 3–6 different mice at each time point. The initial amount was set to 1. **e** Representative Western blot of RyR1 on CTRL and RyR1-Rec quadriceps homogenates at different time points, using myosin heavy chain as a control of protein amount. Statistical analysis: One way ANOVA with Holm-Sidack's test for multiple comparisons

was observed in all the assayed muscles, although the remaining amount slightly differed between the muscles, the highest being in *interosseous* (64% ± 5%) and the lowest in *soleus* (33% ± 5%) (Additional file 1: Fig. S1B).

RyR1-Rec mice show progressive reduction in muscle and body weights and in muscle strength

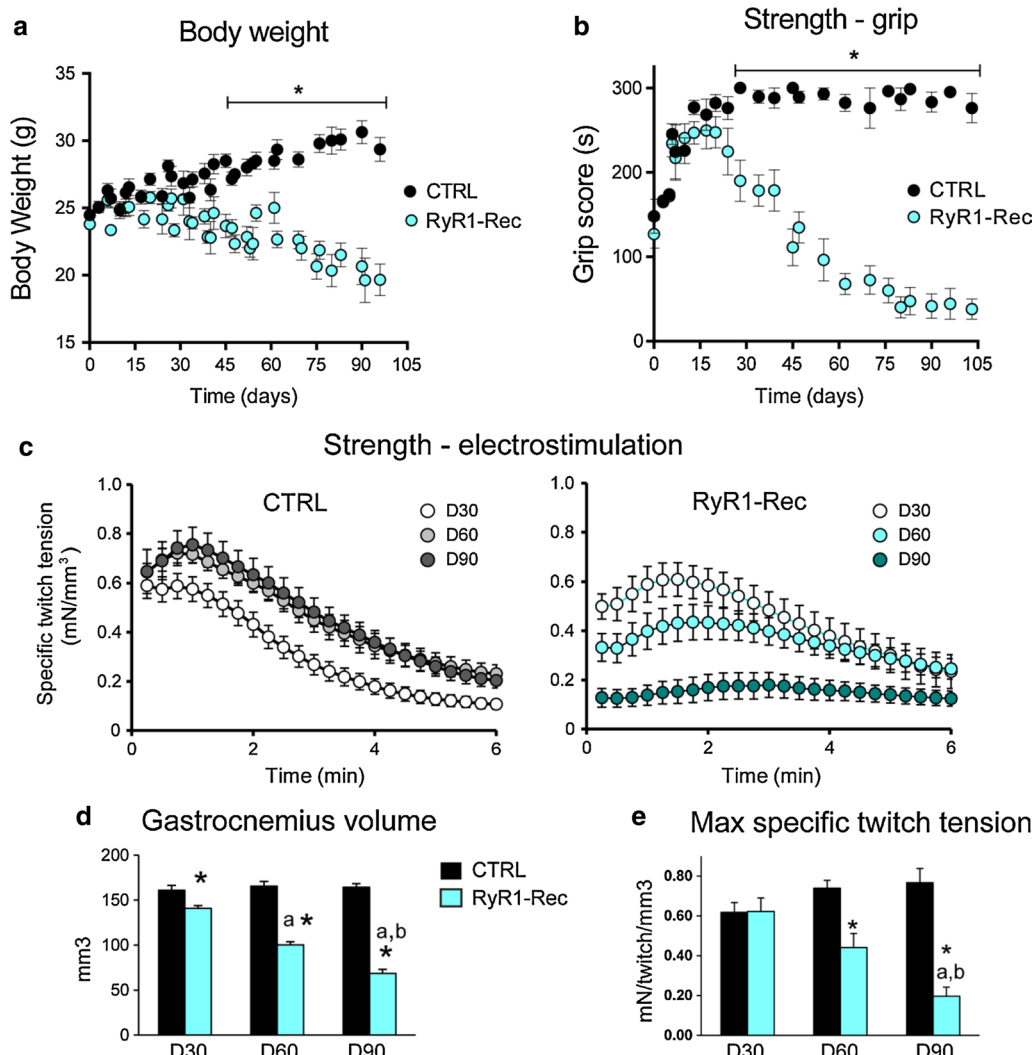The consequences of RyR1 reduction were first studied at the whole animal level. Initially at the same weight, the

Fig. 2 RyR1-Rec mice show progressive reduction in muscle and body weights and in muscle strength. **a** Body weight and **b** Muscle strength estimated as a function of time after recombination using a grip test in which the time the animals can hang upside down on a grid up to 5 min (300 s). Data are mean ± SEM of n = 10-15 animals in each group, *$p < 0.05$ Student's t test with Holm-Sidack's correction for multiple comparisons. **c** Recording of the tension developed by gastrocnemius during a 6 min electrostimulation protocol at 2 Hz. Longitudinal study of the same animals (CRTL, left panel, and RyR1-Rec, right panel) at different times after recombination, 30 days (D30), 60 days (D60) and 90 days (D90). Data are mean ± SEM of n = 8 CRTL and n = 6 RyR1-Rec animals. **d** *Gastrocnemius* muscle volume for CTRL (n = 8) and RyR1-Rec (n = 6) mice at 30, 60 and 90 days after recombination. Data are mean ± SEM. Statistical analysis: post hoc LSD Fisher test following two-way repeated measures ANOVA, *significantly different from CTRL at the same time, [a]significantly different from D30 in the same group, [b]significantly different from D60 in the same group. **e** Maximal specific twitch tension (maximal twitch tension normalized to the gastrocnemius volume). Statistical analysis: post hoc LSD Fisher test following two-way repeated measures ANOVA *significantly different from CTRL at the same time, [a]significantly different from D30 in the same group, [b]significantly different from D60 in the same group

CTRL animals slowly gained weight from 24.4 ± 0.4 to 30.6 ± 0.8 g at D90 whereas the RyR1-Rec animals progressively lost weight to 20.6 ± 1.3 g at D90 (Fig. 2a). Both males and females were affected and lost about 13% of their initial body weight after 75 days (Additional file 1: Fig. S1C). This is the result of a weight loss observed in all the muscles (Additional file 1: Fig. S1D). To test the overall muscle performance after RyR1 reduction, the animals

were subjected to two different strength tests. They were first allowed to hang gripping a cross-wired surface with all four paws up to 5 min, the latency to fall reflecting the muscle force. The grip test performed every week during 105 days (Fig. 2b) showed that RyR1-Rec animals started losing strength 20–30 days after tamoxifen injection, when the amount of RyR1 was about 75–80% of its initial value, and were unable to hang on the grid about 75 days

after tamoxifen injection, as RyR1 amount had reached the level of about 60%. Muscle strength was also assessed by a 6 min noninvasive electrostimulation protocol of the *gastrocnemius* muscle coupled to anatomic magnetic

resonance imaging (MRI) under general anesthesia. During the electrostimulation protocol of CTRL animals 30 days after tamoxifen injection (Fig. 2c, D30) a typical exercise profile was recorded, with a stable initial muscle
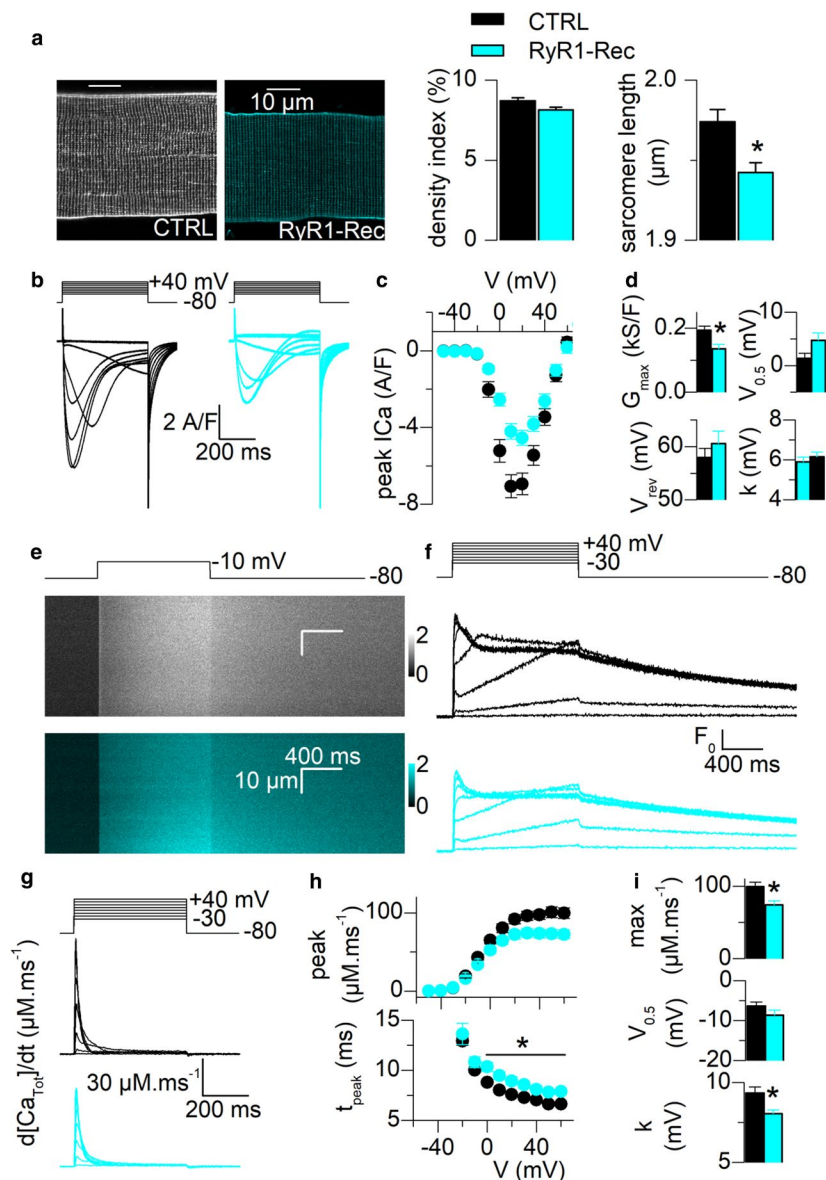

Fig. 3 Excitation-contraction coupling in single isolated muscle fibers is altered. All values are mean ± SEM. Statistical significance was determined using a Student's t-test. **a** Representative confocal images of T-tubule network stained with di-8-anepps from a CTRL and a RyR1-Rec fiber, allowing evaluation of T-tubule density and sarcomere length, performed in 42 CTRL fibers and 41 RyR1-Rec fibers (4 mice in each group). **b** Representative DHPR Ca^{2+} current from a CTRL and a RyR1-Rec fiber in response to 0.5 s-long depolarizing steps to the indicated levels (10 mV increment). **c** Voltage-dependence of the peak DHPR Ca^{2+} current density. **d** Parameters obtained from the fit of curves **c** in 29 CTRL fibers and 30 RyR1-Rec fibers (5 mice in each group), (cf Additional file 1: Supp. Method). **e** Representative *x,t* images of rhod-2 fluorescence (a.u.) from a CTRL and a RyR1-Rec fiber stimulated by a voltage-clamp depolarizing pulse to − 10 mV. **f** Representative line-averaged rhod-2 Ca^{2+} transients from a CTRL and from a RyR1-Rec fiber in response to voltage-clamp pulses to the indicated levels. **g** Rate of SR Ca^{2+} release calculated from the curves shown in **f**. **h** Voltage-dependence of the peak rate of SR Ca^{2+} release (top) and of the time-to-peak rate of SR Ca^{2+} release (bottom). **i** Parameters obtained from fitting the peak rate of SR Ca^{2+} release *vs* voltage relationship with a Boltzmann function in each fiber (cf Additional file 1: Supplementary Method). Data are from the same fibers as in **b**–**d**

strength which slowly declined as muscle fatigued. In the CTRL group at D60 and D90 the exercise profile showed improved muscle force when the animals got older (Fig. 2c). In contrast, the performance of RyR1-Rec animals, similar to CTRL at D30, deteriorated with age. RyR1-Rec animals were unable to perform the exercise anymore at D90 (Fig. 2c, RyR1-Rec D90). *Gastrocnemius* volume measured using MR images (Fig. 2d) remained stable in CTRL animals from D30 (161 ± 5 mm^3) to D90 (164 ± 4 mm^3). In contrast, in RyR1-Rec mice, *gastrocnemius* volume was significantly smaller than in CTRL mice since D30 (141 ± 3 mm^3, $p = 0.003$), and was further reduced down to 100 ± 3 mm^3 at D60 ($p < 0.001$ compared to CTRL at the same age) and 69 ± 4 mm^3 at D90 ($p < 0.001$ compared to CTRL at the same age). The maximal specific twitch tension (absolute twitch tension normalized to muscle volume) confirms that both groups presented similar muscle strength at D30 (Fig. 2e), but RyR1-Rec animals' strength dramatically declined whereas it increased in CTRL animals as they got older. Additionally, the changes in *gastrocnemius* muscle bioenergetics during the electrostimulation were assessed noninvasively at D60 using in vivo 31-phosphorus (^{31}P) MR spectroscopy. Whereas the basal intramyofibrillar pH did not differ between both groups (Additional file 1: Fig. S2A), the extent of acidosis at the end of the exercise was lower ($p = 0.016$) in RyR1 Rec animals (Additional file 1: Fig. S2B), thereby suggesting that glycolytic flux in exercising muscle was reduced in these animals. Moreover, the time constant of post-exercise phosphocreatine resynthesis (τPCr) was significantly shorter ($p = 0.047$) in RyR1-Rec mice (Additional file 1: Fig. S2C, D), reflecting an improved in vivo mitochondrial function. Indeed, PCr synthesis during the post-exercise recovery period relies exclusively on oxidative ATP synthesis, thus τPCr is considered as an index of the oxidative phosphorylation capacity [27]. Overall, these results indicate that RyR1 progressive reduction is associated with a progressive loss of weight and a drop in muscle strength.

The physiological properties of isolated fibers are compromised in RyR1-Rec mice

The alteration of muscle function was further characterized at the single muscle fiber level using a combination of whole-cell voltage-clamp and confocal imaging [24, 25]. The T-tubule network was imaged by staining the plasma membrane with di-8-anepps. No qualitative difference in the network (Fig. 3a, left) or quantitative difference in the mean T-tubule density between CTRL and RyR1-Rec fibers were observed, beside a slight but significant shortening of the mean resting sarcomere length (Fig. 3a, graphs on the right). The voltage-activated Ca^{2+} influx through the DHPR (Fig. 3b–d) and of the Ca^{2+}

release flux through RyR1 (Fig. 3e–i) were simultaneously assessed. As compared to CTRL fibers, RyR1-Rec fibers exhibited voltage-activated DHPR Ca^{2+} currents of similar time course (Fig. 3b) but reduced density, as shown by the peak current density *vs* voltage in the two groups (Fig. 3c), which translated into a 30% reduction in maximum conductance (G$_{max}$) with no associated change in the other parameters of the current *vs.* voltage relationship (Fig. 3d). The voltage dependence of SR Ca^{2+} release was assessed from line-scan imaging of the Ca^{2+}-sensitive dye rhod-2. Line-scan images from the RyR1-Rec fibers were qualitatively similar to those from CTRL fibers (Fig. 3e), showing a rapid rise in fluorescence upon T-tubule membrane depolarization, spatially homogeneous along the scanned line. The rate of SR Ca^{2+} release (Fig. 3g), calculated from the changes in rhod-2 fluorescence elicited by depolarizing pulses of increasing amplitude (Fig. 3f), exhibited a similar time course in RyR1-Rec fiber as in CTRL fibers, but importantly, peak values were reduced in RyR1-Rec. Fitting of the peak rate of SR Ca^{2+} release *vs* voltage (Fig. 3h-top graph) indicated that the maximum rate of Ca^{2+} release was reduced by 25% in the RyR1-Rec group (Fig. 3i, Max), the slope factor (k) was also slightly but significantly reduced, whereas the voltage of mid-activation ($V_{0.5}$) was unchanged. A slight (1.3 ms in average) but significant increase in the time-to-peak rate of SR Ca^{2+} release in the RyR1-Rec fibers (Fig. 3h, bottom graph) was observed. No modifications were observed in the cytosolic Ca^{2+} removal capabilities of the fibers (SERCA pump function), measured with the low-affinity Ca^{2+}-sensitive dye fluo-4 FF in non-EGTA-buffering conditions (Additional file 1: Fig. S3). Overall, these results demonstrate that the 35% reduction in RyR1 amount in *interosseous* is associated with a 30% reduction in calcium current through DHPR and a 25% reduction in calcium flux through RyR1.

RyR1 reduction affects the skeletal muscle structure

To better understand the basis of these functional alterations associated with a decrease in RyR1, muscle structure was studied on RyR1-Rec animals at D75 after recombination, and compared to CTRL animals. *Extensor digitorum longus* (EDL*)*, a fast twitch muscle, *soleus*, a slow twitch muscle and *tibialis anterior* (TA), a mixed muscle were analyzed using hematoxylin–eosin, NADH and Gomori trichrome stainings. Stainings of TA, presented in Fig. 4a, show abnormal muscle structure in RyR1-Rec animals, without fibrosis or central nuclei, but with fiber atrophy, affecting both type I and type II fibers (Table 2). A mitochondria disorganization characterized by local accumulation/depletion in adjacent regions of the same fiber (arrowhead and inset Fig. 4a) and red staining accumulation observed with Gomori trichrome
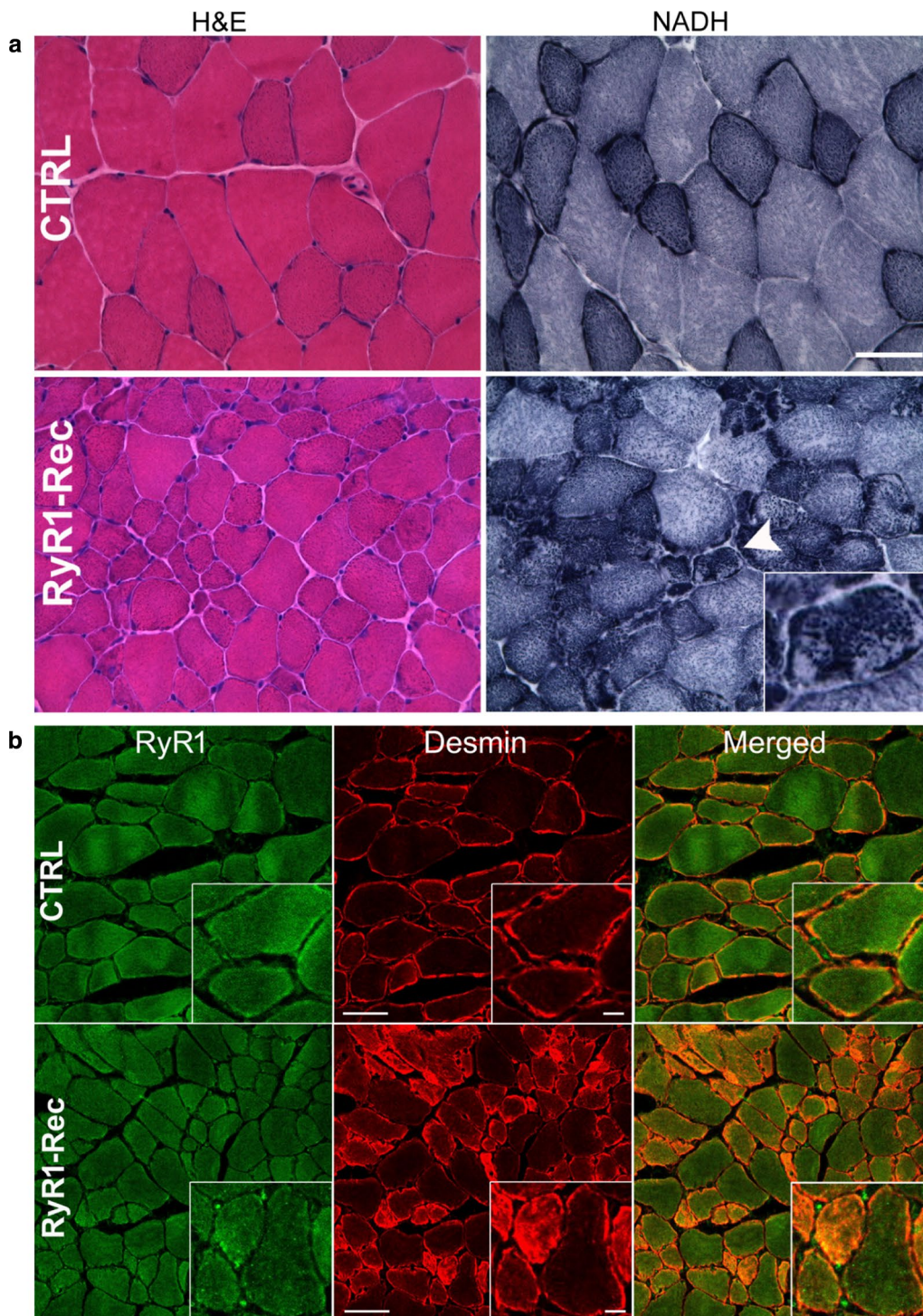
Fig. 4 Histological and immunofluorescent analyses show major defects in muscles. **a** *TA* Transversal section from CTRL and RyR1-Rec mice at D75 were stained with hematoxylin/eosin (H&E) and NADH. The mitochondria localization (NADH staining) is inhomogeneous in RyR1-Rec fibers, specifically in the small dark type I (slow) fibers with high mitochondria content (arrow head and inset). The nuclei (blue dots with H&E staining) are at the periphery of the fibers, and no evidence of regenerative fiber can be seen. Bar 50 μm. **b** Transversal TA sections from D75 CTRL and RyR1-Rec mice were stained with antibodies against RyR1 (green) and desmin (red). Bar 50 μm, and 10 μm in inset

(Additional file 1: Fig. S4) was also observed, resembling the dusty cores recently described in patients [16]. Fiber atrophy was observed in both fiber types in EDL, although the reduction was slightly more important in type I fibers (Table 2). Transversal TA section of CTRL and RyR1-Rec mice were stained with antibodies against RyR1 and desmin. No modification was observed in the RyR1 distribution between type I and type II fibers in RyR1-Rec TA sections, indicating a similar RyR1 reduction in all fiber types (Fig. 4b). Surprisingly, an important modification was observed in desmin distribution, with a huge increase in the small type I fibers (Fig. 4b): in CTRL TA sections, all fibers presented a similar peripheral staining, whereas the small type I fibers in RyR1-Rec TA sections were heavily stained both at the fiber periphery and in the cytosol (inset Fig. 4b). Although IF labelling is not quantitative, these results show that RyR1 reduction was most probably homogenous, without any huge difference between adjacent fibers as observed for desmin, the quantification performed by Western blot being the reflect of protein contained in each fiber and not a mean of fibers with 0% RyR1 and fibers with 100% RyR1 within the same muscle.

Triads organization was further studied using immunofluorescent labelling of isolated EDL fibers (Fig. 5a). The labeling of alpha-actinin (as a marker of the Z-line), of triadin and of RyR1 (as triad markers) on RyR1-Rec EDL fiber demonstrated that the reduction in RyR1 amount resulted in a generalized disorganization of the fiber with abnormal triads localization and disruption of the Z-line, but triadin and RyR1 were still partially colocalized. Although triads remained on both sides of the Z-line, the Z-line did not form a straight line as in CTRL and instead presented many micro-disruptions (inset Fig. 5a). Muscle ultrastructure was analyzed using electron microscopy on RyR1-Rec EDL fibers at D75 (Fig. 5b). Some regions had a relatively preserved structure (Fig. 5b, left fiber), whereas some adjacent regions were highly disorganized, with disruption of sarcomere regular organization, mitochondria disorganization, and

the presence of numerous stacks of membrane (Fig. 5b, arrows, enlarged in inset), previously called multiple triads [16, 28]. The morphological features of those multiple triads compared to the normal single triads are presented in Table 3, and additional examples are presented in Additional file 1: Fig. S5. Precise quantification of putative T-tubule width, putative SR width and intermembrane (T-tubule/SR) space (Additional file 1: Fig. S5) demonstrated a huge increase in the T-tubule mean size in those multiples triads (twofold increase, reaching 202% of the T-tubule size in normal triad), whereas the SR mean width was only slightly increased ($+10\%$) and the intermembrane space was not modified. Those results point to a generalized structural disorganization of RyR1-Rec mice muscles associated with membranes remodeling.

RyR1 reduction is associated with modification in the amount of numerous proteins

The consequences of RyR1 reduction were studied at the molecular level using quantitative Western blot on quadriceps muscle of CTRL or RyR1-Rec mice (8 animals in each group) at D75 after tamoxifen injection (Fig. 6). The relative amount of numerous proteins involved directly or indirectly in calcium handling was estimated, using as reference the total amount of proteins determined by stain free evaluation [29]. No difference in the quantification of RyR1 was observed between this method and the use of myosin heavy chain as a reference protein (comparison between Figs. 1, 6). No significant modification between CRTL and RyR1-Rec muscles was observed in the amount of the triadin isoform T95, the calcium binding protein CSQ1, the Ca^{2+}-ATPase SERCA, the mitochondrial FoF_1-ATPase, and the alpha 1 subunit of DHPR (Fig. 6a, b). In contrast, an increase was observed in the amount of STIM1 ($\times 3.7 \pm 1$, $p = 0.02$), the triadin isoform T51 ($\times 1.6 \pm 0.1$, $p < 0.001$), CLIMP63 ($\times 1.8 \pm 0.2$, $p = 0.004$), and ORAI1 ($\times 3.7 \pm 1$, $p = 0.017$). As modification in the localization of the structural protein desmin was observed using immunofluorescent

Table 2 Analysis of muscle fibers' diameter

	CTRL diameter (µm)	SEM	Nb fiber	RyR1-Rec diameter (µm)	SEM	Nb fiber	Student *t*-test	%CTRL
EDL type I	23.6	0.9	700	17.2	0.7	700	*p* < 0.001*	73
EDL type II	40.0	1.6	600	32.5	1.2	700	*p* < 0.001*	81
TA type I	33.7	1.9	300	20.0	1.2	300	*p* < 0.001*	59
TA type II	46.8	2.7	300	35.6	2.1	300	*p* < 0.001*	76

The diameter of slow (type I) and fast (type II) fibers was quantified in *Extensor digitorum longus* (EDL) and *tibialis anterior* (TA) sections of CRTL and RyR1-Rec animals at D75 after NADH-TR staining. Hundred fibers were measured for each muscle. Between 3 and 7 mice in each group
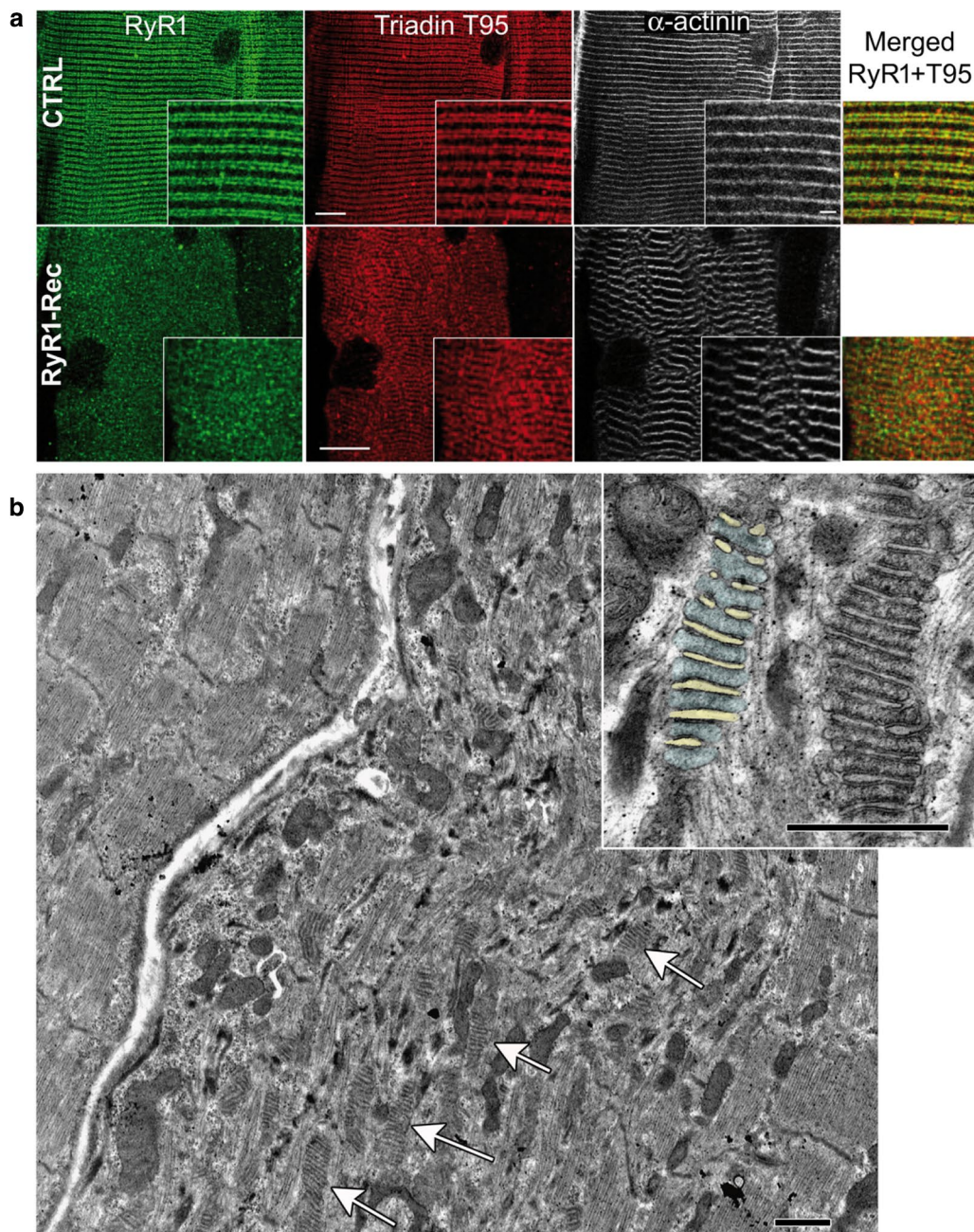
*Represent significant data

Fig. 5 A generalized structural disorganization is observed in EDL muscle fibers. **a** EDL fibers from D75 CTRL and RyR1-Rec mice were stained with antibodies against RyR1 (green), triadin (red) and alpha-actinin (white). Bar 10 μm and 2 μm in inset. **b** Electron microscopy analysis of longitudinal *EDL* section of D75 RyR1-Rec mice. The upper left fiber has a normal structure, the adjacent lower fiber is extremely disorganized, with large stacks of membranes (up to 15 stacks, arrows) extending on few μm long. The inset presents two multiple triads, on the left one the membranes corresponding to T-tubules have been colored with light yellow and the SR sheets with light blue to allow a better visualization. Some electron dense material can be seen within the SR segment, all along the contact site with the adjacent T-tubule, which could correspond to accumulation of proteins. Bars 1 μm

labeling (Fig. 5b), desmin expression level was also quantified and a huge increase in desmin amount was observed ($\times 8.2 \pm 1.2$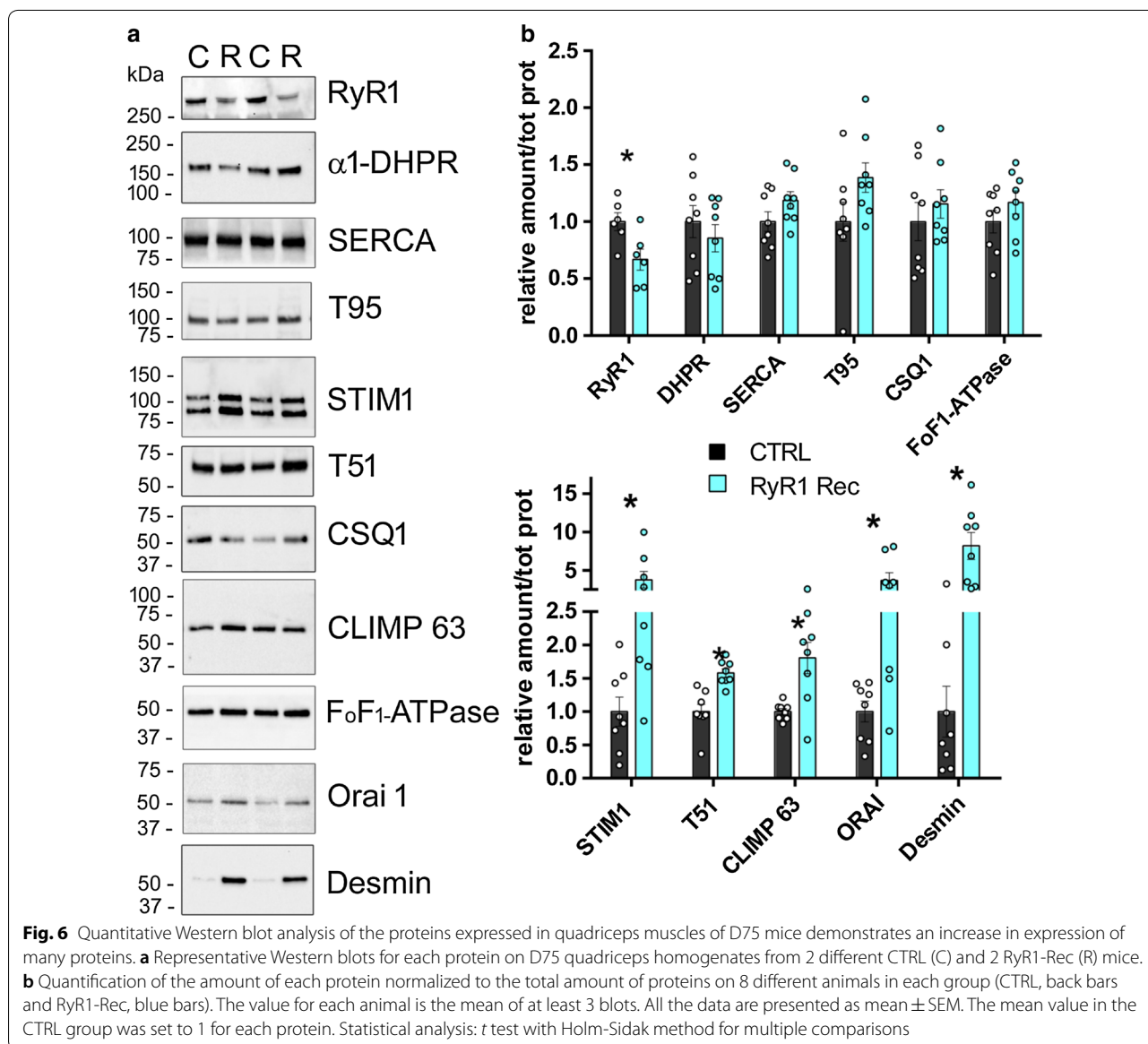, $p = 0.001$). The localization of CLIMP63 and STIM1 in RyR1-Rec EDL fibers was analyzed using immunofluorescent labeling, and no major modification was observed (Additional file 1: Fig. S6).

Table 3 Morphological characterization of single and multiple triads

	Single (CTRL)			Multiple (RyR1-Rec)			Student *t* test	% CTRL
	Mean	SEM	n	Mean	SEM	n		
TT width (nm)	26.0	0.5	140	52.7	1.6	135	$p < 0.001$*	202
SR width (nm)	77.5	0.8	239	85.2	1.2	107	$p < 0.001$*	110
SR-TT space (nm)	20.6	0.3	135	20.5	0.4	138	0.9	100

The size of T-tubules, SR and intermembranes space thickness were measured as presented on Additional file 1: Fig. S5

*Represent significant data

Fig. 6 Quantitative Western blot analysis of the proteins expressed in quadriceps muscles of D75 mice demonstrates an increase in expression of many proteins. **a** Representative Western blots for each protein on D75 quadriceps homogenates from 2 different CTRL (C) and 2 RyR1-Rec (R) mice. **b** Quantification of the amount of each protein normalized to the total amount of proteins on 8 different animals in each group (CTRL, back bars and RyR1-Rec, blue bars). The value for each animal is the mean of at least 3 blots. All the data are presented as mean ± SEM. The mean value in the CTRL group was set to 1 for each protein. Statistical analysis: *t* test with Holm-Sidak method for multiple comparisons

Therefore RyR1 protein reduction was associated with an increase in different proteins involved in calcium regulation or in muscle architecture.

Autophagy is altered as a result of RyR1 reduction

Alteration in autophagy has been observed in some myopathies [30, 31]. In order to identify the mechanisms

leading to the muscle atrophy subsequent to RyR1 reduction, we looked for modifications in the autophagy flux in RyR1-Rec muscles. The amount of LC3 II, a membrane protein of the autophagosomes, was evaluated with quantitative Western blot (Fig. 7a, b), and an increase in LC3 II was observed ($172\% \pm 32\%$, $p = 0.03$). This increase in autophagosomes could reflect either an increase in formation of autophagosomes (due to an increase in autophagy process) or a decrease in their fusion with lysosomes (and therefore an inhibition of autophagy degradation). The precise nature of autophagy flux modification was further analyzed by quantification of p62, a well-known protein specifically degraded via autophagy, which amount was also significantly increased (Fig. 7a, b, $172\% \pm 22\%$, $p = 0.006$). The associated increase in LC3 II and in p62 in RyR1-Rec muscle compared to control suggested that RyR1 reduction was therefore associated with inhibition of the autophagy flux. Moreover, an increase in the activation (phosphorylation) of two inhibitors of autophagy, mTOR and S6 protein (Fig. 7b, c), was observed (P-mTOR/mTOR increase by $174\% \pm 17\%$, $p = 0.01$; P-S6/S6 increase by $320\% \pm 50\%$, $p < 0.001$). The increase in the phosphorylation of these two autophagy inhibitors in RyR1-Rec animals compared to controls further pointed towards an inhibition of autophagy responsible for the muscle atrophy in RyR1-Rec animals.

Human patients' biopsies exhibit similar defects to those observed in RyR1-Rec mice

In a recent study on a large cohort of patients with a recessive congenital myopathy [16], we have identified the presence of atypical structures, called "dusty cores", in more than half of the patients with a reduction in RyR1 amount. They were observed by multiple staining and differ from the classical central core (well defined regions devoid of oxidative stain) by their poorly defined borders, their focal myofibrillar disorganization, a reddish-purple granular material deposition at Gomori trichrome staining and blended area with decreased or/and increased enzymatic activity at oxidative stains [16] (Additional file 1: Fig. S7). These structural alterations mirror the modifications observed in our mouse model (Fig. 4 and Additional file 1: Fig. S7). We therefore further compared our new mouse model and muscle biopsies from patients with a RyR1 protein reduction and "dusty cores". Using quantitative Western blot, the amount of the proteins which were clearly modified in our mouse model was also estimated in 5 patients with a recessive Dusty Core disease (two RyR1 mutations resulting in RyR1 protein reduction—Fig. 8a). Control biopsies of different age (between 3.5 and 64 years) were used as reference. A large reduction in RyR1 protein was observed in all the patients (mean

expression level $19.8\% \pm 2.2\%$ of CTRL, $p < 0.001$). Moreover, an increase in CLIMP63 and desmin was also observed. The reduction in RyR1 was associated with an important increase in CLIMP 63 (mean expression level increase fivefolds, $516\% \pm 220\%$). In addition, the expression level of desmin was also drastically increased in patients compared to control (mean expression level increase 240-folds, $24\ 170\% \pm 7\ 635\%$). Using electron microscopy to analyze patient biopsy's ultrastructure, many stacks of membranes were observed in the disorganized regions (Fig. 8c, arrows) of all the patients. These regions, similar to the stacks observed in RyR1-Rec muscle (Fig. 4b), pointed to a common mechanism, both in mice and in human, leading to the formation of those structures as a result of RyR1 reduction. With identical modifications as the ones in Dusty Core Disease patients, this model constitutes thus a relevant model to study the pathophysiological mechanisms.

Discussion

We present here the first model of mice with a clear myopathy phenotype due to the exclusive reduction in the expression of the *RYR1* gene. Two mouse models with recessive RyR1 mutations have been recently published, with an hypomorphic allele combined with a point mutation [11, 12], but in these models, the reduction in RyR1 amount being associated to the expression of a mutant channel with altered calcium permeability, it not possible to discriminate the effects related to reduction in protein to the effects of abnormal channel expression. The common features observed in those two models and the one described here allow now to identify the underlying pathophysiological mechanisms and to attribute these features to RyR1 reduction.

The recombination of the *RYR1* gene in this inducible and muscle specific RyR1-KO mouse line was performed at the adult stage, and induced a progressive reduction in RyR1 protein amount in adult and well-structured muscles, thus avoiding possible developmental effects of *RYR1* knockdown. Although the production of *RYR1* transcript was rapidly shut down and plateaued at a low and stable level (fivefold reduction after 5–7 days), RyR1 protein reduction was much slower and incomplete, being reduced by 50% only after 90 days, without further modification. This could reflect a stability of RyR1 protein to an unknown extent although in vivo experiments with radioactive labeling in rat muscle suggested a turnover of 8–10 days [32, 33]. Such a long stability was observed for the alpha 1 subunit of DHPR, which was knocked down with a U7-exon skipping strategy that resulted only in a 50% reduction of the protein level after 2–6 months, in
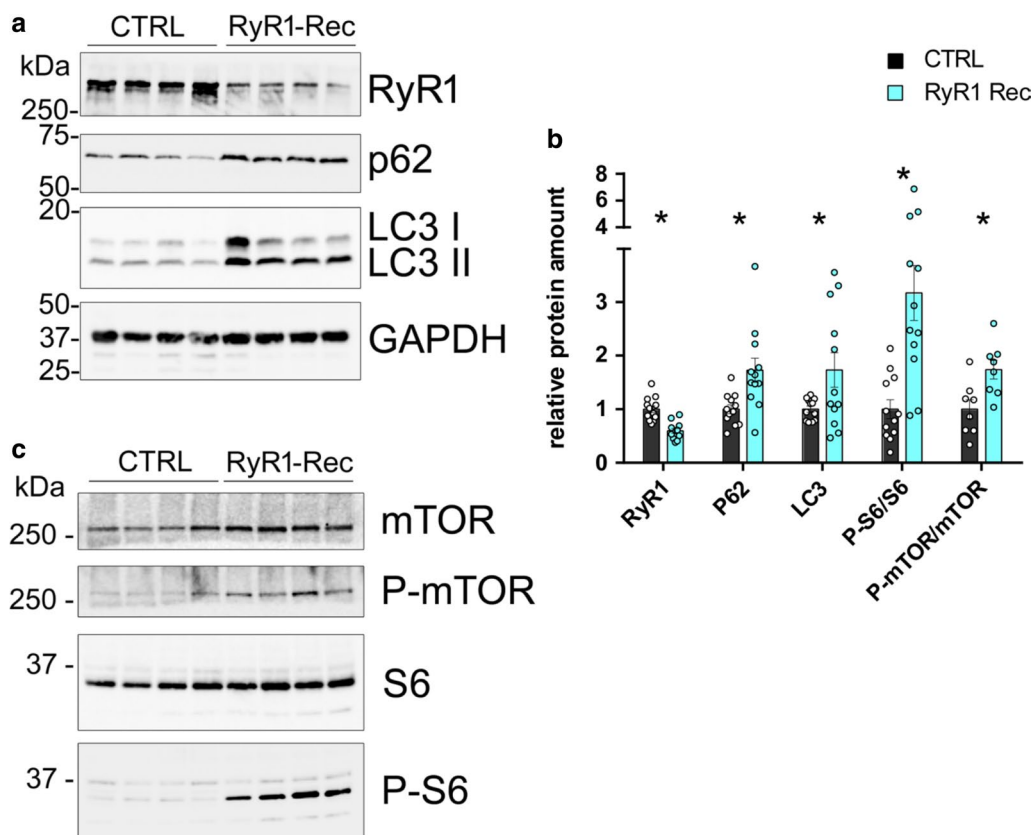
Fig. 7 Autophagy is inhibited in RyR1-Rec D75 mice quadriceps muscle. **a**, **c** Representative Western blot on 4 CTRL and 4 RyR-Rec quadriceps muscle homogenates. **b** Quantification of the amount of protein normalized to the amount of GAPDH in 8–12 mice in each group (CTRL, black bars; RyR1-Rec, blue bars). For S6 and mTOR, the values are presented as ratio of the phosphorylated/non-phosphorylated protein. The value for each animal is the mean of at least 3 blots. All the data are presented as mean ± SEM. The mean value in the CTRL group was set to 1 for each protein. Statistical analysis: *t* test with Holm-Sidak method for multiple comparisons

presence of a remaining amount of 10–20% at the mRNA level [34].

The progressive reduction in RyR1 amount in our mouse line was associated with a progressive reduction in muscle strength, as evidenced by the direct measurement of the spontaneous ability of the animals to hang on a grid or by the evaluation of muscle tension developed during muscle electrostimulation. Our results suggest a direct correlation between the amount of RyR1 protein and the muscle strength. In our model, almost no muscle weakness was observed when RyR1 amount was above 80% of control, as already observed with the heterozygous whole body RyR1-KO mice that showed a RyR1 protein amount of 85% of control and no functional alteration [15]. The drop in muscle strength in RyR1-Rec animals parallels protein amount, and when RyR1 amount reached 50% of control, the animals were unable to perform any of the two tests (hanging or electrostimulation). The direct study of DHPR and RyR1 function on isolated fiber demonstrated a reduction in the function of

both calcium channels. The reduction in RyR1-calcium release activity was of 25%, which is similar to the reduction in RyR1 protein in the specific muscle used for the experiment (*interosseous* muscle). Interestingly, a similar correlation between the amplitude of calcium release and the amount of RyR1 has been observed in the two recent recessive RyR1 mouse models [11, 12], with a 50% reduction in calcium release associated to a 65% reduction in protein amount [12]. Surprisingly, no modification in DHPR amount or in the T-tubule density was observed, although calcium influx through DHPR was reduced by 30%. This could reflect the so-called retrograde coupling [35] by which RyR1 controls DHPR function, as observed in the RyR1-KO cells with DHPR functional alteration [36].

At the structural level, all muscles were affected, and both type I (slow) and type II (fast) fibers were atrophied without any sign of basal membrane detachment (which would have reflected denervation), and with alteration in mitochondria distribution in type I fibers. A generalized
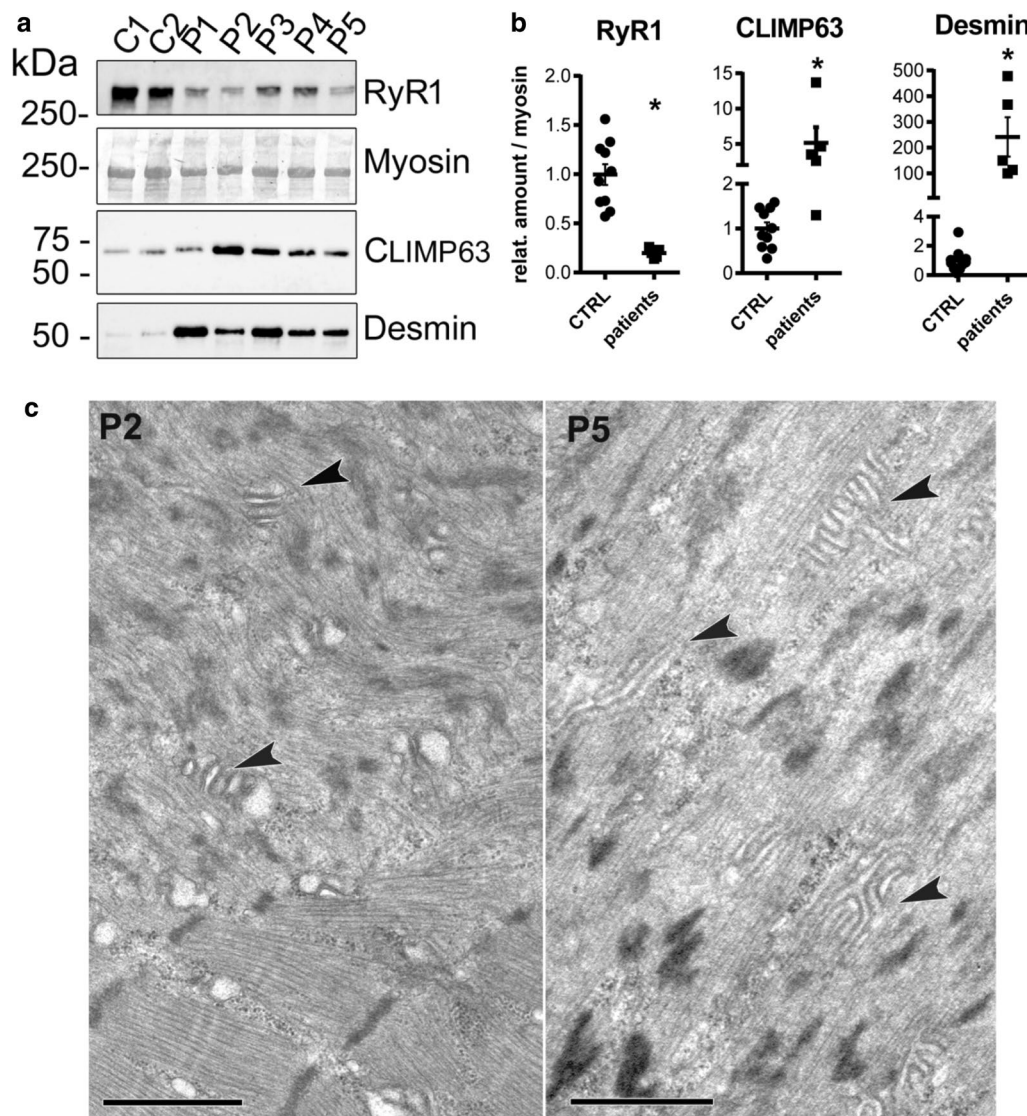
Fig. 8 Analysis of human patients' biopsies reveals similar defects to those observed in RyR1-Rec mice. **a** Representative Western blot performed on muscle homogenate from human biopsies. C1: control, 23 years, female; C2: control, 3.5 years, male; P1: CCD (Dusty core), mutations p.M2423K + p. R2441*, 43 years, male; P2: CCD (Dusty core), mutations p.T4709M + p.R1409*, 4 years, male; P3: CCD (Dusty core), mutations p.[Ile1571Val; Arg3366His; Tyr3933Cys] + p.Val788Cysfs*96, 25 years, female; P4: CCD (Dusty Core), mutations p.R2140W + p.L4828R, 9 years, female; P5: CCD (Dusty Core), mutations p.M4000del + p.Met2312Cysfs*118, 28 years, female. **b** Quantification of protein amount, normalized to myosin (for RyR1, CLIMP63 and Desmin) or to GAPDH (for p62). Data are presented as mean ± SEM of 10 controls samples (CTRL) and of 5 patients' samples (patients). The value for each patient is the mean of at least 2 Western blots. The mean value for each protein in CTRL samples was set to 1. RyR1 expression level compared to controls: P1—26 ± 6%, P2—14 ± 6%, P3—20 ± 3%, P4—23 ± 3%, P5—16 ± 2%. CLIMP63 expression level compared to control: P1—130% ± 12%, P2—1372% ± 385%, P3—466% ± 92%, P4—262% ± 35%, P5—350% ± 85%). Desmin expression level compared to control: P1—47,789% ± 6097%; P2—10,052% ± 2957%; P3—36,745% ± 7150%; P4—14,951% ± 5584%; P5—11,307% ± 2858%. Student *t* test RyR1 $p < 0.001$, CLIMP63 $p = 0.016$, Desmin $p < 0.001$ **c** Electron microscopy pictures obtained during the course of the diagnosis, presenting multiples stacks of membranes in the disorganized core region of the biopsies of patients P2 and P5. Similar structures were identified in the muscle biopsies of the five patients. Bar 1 µm

disorganization of muscle structure was observed in most fibers with variable severity, from almost normal muscle structure to focal highly disorganized regions. In those highly disorganized regions, resembling the core lesions in patients, disruption of the regular alignment of the sarcomeres with abnormal mitochondria and triad localizations were observed, and the most striking feature was the presence of numerous and large stacks of membrane.

Those membrane stacks, hypothetically corresponding to the close alternate apposition of SR and T-tubules, were called multiple triads [16], but the exact nature of each membrane type remains to be determined. Similar structures have been observed in muscle of CSQ1-KO mice [28], although smaller. The size of the SR sheets in those multiple triads is similar to the size of the SR terminal cisternae in regular triads, but the T-tubules are dilated and twice the normal size. Careful examination of those multiple triads did not allow the identification of "feet", those electron dense structures formed by RyR1 [37] between SR and T-tubule membranes. So these stacks of membranes are most likely depleted of RyR1. Space size between SR and T-tubule is similar in multiple triads and in the regular triads, thus the proteins involved in the assembly of those structures are probably the same. As the RyR1 staining is uniform on transversal section, RyR1 depletion occurred most likely in all fiber types, although desmin overexpression and delocalization has been seen mainly in type I fibers.

At the molecular level, some important modifications were observed, such as a twofold to threefold increase in CLIMP63 and in STIM1, and a massive increase in desmin ($\times 80$). The mechanisms connecting the structural disorganizations with the overexpression of desmin, CLIMP63, STIM1 are still unclear, and require further analysis. Those modifications, both at the structural and protein levels, have been observed in mice and in human patients with RyR1 mutations resulting only in RyR1 reduction, pointing to a common pathophysiological mechanism between mouse and human. Desmin forms intermediate filaments involved in the muscle cell architecture by anchoring several structures (nucleus, mitochondria, Z-disc) to the plasma membrane at the costamers [38, 39], and alterations in desmin result in myopathies [40]. Desmin overexpression could reflect a direct regulation of the desmin gene by the calcium released from the sarcoplasmic reticulum. On the other hand, desmin aggregation and mislocalization leading to muscle weakness could contribute to the overall phenotype observed both in mice and in patients with RyR1 reduction. CLIMP63 is a reticulum protein, associated with the calcium release complex via its interaction with triadin [19], which is involved in the shaping of reticulum membrane and in the formation of reticulum sheets [41]. Its overexpression observed both in mice and in patients with RyR1 reduction could be associated with (and perhaps responsible for) the formation of the multiple triads observed in both cases. Along the same line, STIM1 is not only involved in the refilling of calcium stores via its interaction with ORAI1, but also in the reticulum morphogenesis via its interaction with the microtubule +TIP binding protein EB1 [41], pointing to its possible

involvement in the formation of those multiple triads. As ORAI1 undergoes the same magnitude of overexpression as STIM1, it is mostly likely that the two proteins still work together, but the functional consequences of this overexpression on the calcium entry activated by store depletion (SOCE) has to be demonstrated. The overexpression of STIM1 and ORAI1 has already been associated with SR and T-tubule remodeling during exercise [42, 43], resulting in the formation of stacks of few (2–4) SR membranes associated with a T-tubule, with a gap between both being smaller than the normal triadic gap. The structures observed in RyR1 deficient mouse muscle looked similar although much larger (up to 15 stacks of each membrane), and with a clear alternation of two membrane types but with the same space size between the membranes. Inhibition of autophagy has been evidenced in mice, which could explain the muscle atrophy observed, as both increase or decrease in autophagy have been described as leading to muscle atrophy [44].

Conclusions

To conclude, this study demonstrates that RyR1 reduction is sufficient to induce a myopathy. This model recapitulates the main features observed in "Dusty core Disease" patients, a subgroup of Central Core Disease with exclusive RyR1 reduction, and due to a better homogeneity between the mice (same age, same sex, …) than between the patients (different severity, different age at the biopsy, different age at onset of the disease, …) and to the higher number of sample available, this mouse model has allowed to point to modifications that could shed a new light on the pathophysiological mechanisms, only partially known, and provide new clues for therapeutic development.

Supplementary information

Supplementary information accompanies this paper at https://doi.org/10.1186/s40478-020-01068-4

> **Additional file 1.** Supplementary method and supplementary figures S1-S7.

Availability of data and materials
The datasets used and/or analyzed during the current study available from the corresponding author on reasonable request.

Ethics approval
All procedures using animals were approved by the institutional ethics committee (CEEA-GIN 04, N_134) and followed the guidelines from Directive 2010/63/EU of the European Parliament on the protection of animals used for scientific purposes. Experimental procedures for human studies were approved by the institutional ethics committee and performed in accordance with ethical standards laid down in the Declaration of Helsinki. All biopsies were collected following informed consent.

Consent for publication
Not applicable.

Competing interests
The authors declare that they have no competing interests.

Author details
[1] INSERM, GIN-U1216, CHU Grenoble Alpes, Grenoble Institut Neurosciences, University Grenoble Alpes, Bat EJ Safra, Chemin Fortuné Ferrini, La Tronche, Grenoble, France. [2] CNRS, CRMBM, Aix-Marseille Univ, Marseille, France. [3] CNRS UMR5310, INSERM U1217, Institut NeuroMyoGene, University Lyon I, Lyon, France. [4] CNRS UMR7104, INSERM U1258, Institut de Génétique et de Biologie Moléculaire et Cellulaire, University Strasbourg, Illkirch, France. [5] Department of Cell and Developmental Biology, University of Pennsylvania, Philadelphia, PA, USA. [6] Neuromuscular Morphology Unit, Center for Research in Myology, Myology Institute, Sorbonne University, GH Pitié-Salpêtrière, Paris, France.

References
1. Marty I, Robert M, Villaz M, Lai Y, De Jongh KS, Catterall WA et al (1994) Biochemical evidence for a complex involving dihydropyridine receptor and ryanodine receptor in triad junctions of skeletal muscle. Proc Natl Acad Sci USA 91:2270–2274. https://doi.org/10.1073/pnas.91.6.2270
2. Zhang L, Kelley J, Schmeisser G, Kobayashi YM, Jones LR (1997) Complex formation between junctin, triadin, calsequestrin, and the ryanodine receptor. Proteins of the cardiac junctional sarcoplasmic reticulum membrane. J Biol Chem 272:23389–23397. https://doi.org/10.1074/jbc.272.37.23389
3. Dirksen RT, Avila G (2002) Altered ryanodine receptor function in central core disease: leaky or uncoupled Ca(2+) release channels? Trends Cardiovasc Med 12:189–197. https://doi.org/10.1016/s1050-1738(02)00163-9
4. Betzenhauser MJ, Marks AR (2010) Ryanodine receptor channelopathies. Pflugers Arch 460:467–480. https://doi.org/10.1007/s00424-010-0794-4
5. Lanner JT, Georgiou DK, Joshi AD, Hamilton SL (2010) Ryanodine receptors: structure, expression, molecular details, and function in calcium release. Cold Spring Harb Perspect Biol 2:a003996. https://doi.org/10.1101/cshperspect.a003996
6. MacLennan DH, Zvaritch E (2011) Mechanistic models for muscle diseases and disorders originating in the sarcoplasmic reticulum. Biochim Biophys Acta 1813:948–964. https://doi.org/10.1016/j.bbamcr.2010.11.009
7. Marty I, Fauré J (2016) Excitation-contraction coupling alterations in myopathies. J Neuromusc Dis 3:443–453. https://doi.org/10.3233/JND-160172
8. Jungbluth H, Treves S, Zorzato F, Sarkozy A, Ochala J, Sewry C et al (2018) Congenital myopathies: disorders of excitation-contraction coupling and muscle contraction. Nat Rev Neurol 14:151–167. https://doi.org/10.1038/nrneurol.2017.191
9. Chelu MG, Goonasekera SA, Durham WJ, Tang W, Lueck JD, Riehl J et al (2006) Heat- and anesthesia-induced malignant hyperthermia in an RyR1 knock-in mouse. FASEB J 20:329–330. https://doi.org/10.1096/fj.05-4497fje
10. Zvaritch E, Kraeva N, Bombardier E, McCloy RA, Depreux F, Holmyard D et al (2009) Ca2+ dysregulation in Ryr1(I4895T/wt) mice causes congenital myopathy with progressive formation of minicores, cores, and nemaline rods. Proc Natl Acad Sci USA 106:21813–21818. https://doi.org/10.1073/pnas.0912126106
11. Brennan S, Garcia-Castañeda M, Michelucci A, Sabha N, Malik S, Groom L et al (2019) Mouse model of severe recessive RYR1-related myopathy. Hum Mol Genet 28:3024–3036. https://doi.org/10.1093/hmg/ddz105
12. Elbaz M, Ruiz A, Bachmann C, Eckhardt J, Pelczar P, Venturi E, Lindsay C et al (2019) Quantitative RyR1 reduction and loss of calcium sensitivity of RyR1Q1970fsX16+A4329D cause cores and loss of muscle strength. Hum Mol Genet 28:2987–2999. https://doi.org/10.1093/hmg/ddz092
13. Elbaz M, Ruiz A, Eckhardt J, Pelczar P, Muntoni F, Boncompagni S et al (2019) Quantitative reduction of RyR1 protein caused by a single-allele frameshift mutation in RYR1 ex36 impairs the strength of adult skeletal muscle fibres. Hum Mol Genet 28:1872–1884. https://doi.org/10.1093/hmg/ddz025
14. Takeshima H, Iino M, Takekura H, Nishi M, Kuno J, Minowa O et al (1994) Excitation-contraction uncoupling and muscular degeneration in mice lacking functional skeletal muscle ryanodine-receptor gene. Nature 369:556–559. https://doi.org/10.1038/369556a0
15. Cacheux M, Blum A, Sébastien M, Wozny AS, Brocard J, Mamchaoui K et al (2015) Functional characterization of a Central Core Disease RyR1 mutation (p. Y4864H) associated with quantitative defect in RyR1 protein. J. Neuromusc Dis 2:421–432. https://doi.org/10.3233/JND-150073
16. Garibaldi M, Rendu J, Brocard J, Lacene E, Fauré J, Brochier G et al (2019) 'Dusty core disease' (DuCD): expanding morphological spectrum of RYR1 recessive myopathies. Acta Neuropathol Commun 7:3. https://doi.org/10.1186/s40478-018-0655-5
17. Schuler M, Ali F, Metzger E, Chambon P, Metzger D (2005) Temporally controlled targeted somatic mutagenesis in skeletal muscles of the mouse. Genesis 41:165–170. https://doi.org/10.1002/gene.20107
18. Marty I, Thevenon D, Scotto C, Groh S, Sainnier S, Robert M et al (2000) Cloning and characterization of a new isoform of skeletal muscle triadin. J Biol Chem 275:8206–8212. https://doi.org/10.1074/jbc.275.11.8206
19. Osseni A, Sébastien M, Sarrault O, Baudet M, Couté Y, Fauré J et al (2016) Triadin and CLIMP-63 form a link between triads and microtubules in muscle cells. J Cell Sci 129:3744–3755. https://doi.org/10.1242/jcs.188862
20. Moutin MJ, Cuillel M, Rapin C, Miras R, Anger M, Lompré AM et al (1994) Measurements of ATP binding on the large cytoplasmic loop of the sarcoplasmic reticulum Ca(2+)-ATPase overexpressed in *Escherichia coli*. J Biol Chem 269:11147–11154
21. Lunardi J, Dupuis A, Frobert Y, Grassi J, Vignais PV (1989) Exploration of delta-subunit interactions in beef heart mitochondrial F1-ATPase by monoclonal antibodies. FEBS Lett 245:223–228. https://doi.org/10.1016/0014-5793(89)80226-1
22. Oddoux S, Brocard J, Schweitzer A, Szentesi P, Giannesini B, Brocard J et al (2009) Triadin deletion induces impaired skeletal muscle function. J Biol Chem 284:34918–34929. https://doi.org/10.1074/jbc.M109.022442
23. Giannesini B, Vilmen C, Le Fur Y, Dalmasso C, Cozzone PJ, Bendahan D (2010) A strictly noninvasive MR setup dedicated to longitudinal studies of mechanical performance, bioenergetics, anatomy, and muscle recruitment in contracting mouse skeletal muscle. Magn Reson Med 64:262–270. https://doi.org/10.1002/mrm.22386
24. Lefebvre R, Pouvreau S, Collet C, Allard B, Jacquemond V (2014) Whole-cell voltage clamp on skeletal muscle fibers with the silicone-clamp technique. Methods Mol Biol 1183:159–170. https://doi.org/10.1007/978-1-4939-1096-0_9
25. Kutchukian C, Lo Scrudato M, Tourneur Y, Poulard K, Vignaud A, Berthier C et al (2016) Phosphatidylinositol 3-kinase inhibition restores Ca2+ release defects and prolongs survival in myotubularin-deficient mice. Proc Natl

Acad Sci USA 113:14432–14437. https://doi.org/10.1073/pnas.1604099113

26. Kutchukian C, Szentesi P, Allard B, Trochet D, Beuvin M, Berthier C et al (2017) Impaired excitation-contraction coupling in muscle fibres from the dynamin2^{R465W} mouse model of centronuclear myopathy. J Physiol 595:7369–7382. https://doi.org/10.1113/JP274990

27. Kemp GJ, Hands LJ, Ramaswami G, Taylor DJ, Nicolaides A, Amato A et al (1995) Calf muscle mitochondrial and glycogenolytic ATP synthesis in patients with claudication due to peripheral vascular disease analysed using 31P magnetic resonance spectroscopy. Clin Sci (Lond) 89:581–590. https://doi.org/10.1042/cs0890581

28. Paolini C, Quarta M, Nori A, Boncompagni S, Canato M, Volpe P et al (2007) Reorganized stores and impaired calcium handling in skeletal muscle of mice lacking calsequestrin-1. J Physiol 583:767–784. https://doi.org/10.1113/jphysiol.2007.138024

29. Gürtler A, Kunz N, Gomolka M, Hornhardt S, Friedl AA, McDonald K et al (2013) Stain-free technology as a normalization tool in Western blot analysis. Anal Biochem 433:105–111. https://doi.org/10.1016/j.ab.2012.10.010

30. Durieux AC, Vassilopoulos S, Lainé J, Fraysse B, Briñas L, Prudhon B et al (2012) A centronuclear myopathy-dynamin 2 mutation impairs autophagy in mice. Traffic 13:869–879. https://doi.org/10.1111/j.1600-0854.2012.01348.x

31. Al-Qusairi L, Prokic I, Amoasii L, Kretz C, Messaddeq N, Mandel JL et al (2013) Lack of myotubularin (MTM1) leads to muscle hypotrophy through unbalanced regulation of the autophagy and ubiquitin-proteasome pathways. FASEB J 27:3384–3394. https://doi.org/10.1096/fj.12-220947

32. Ferrington DA, Krainev AG, Bigelow DJ (1998) Altered turnover of calcium regulatory proteins of the sarcoplasmic reticulum in aged skeletal muscle. J Biol Chem 273:5885–5891. https://doi.org/10.1074/jbc.273.10.5885

33. Martonosi A, Halpin RA (1972) Sarcoplasmic reticulum. XVII. The turnover of proteins and phospholipids in sarcoplasmic reticulum membranes. Arch Biochem Biophys 152:440–450. https://doi.org/10.1016/0003-9861(72)90237-8

34. Piétri-Rouxel F, Gentil C, Vassilopoulos S, Baas D, Mouisel E, Ferry A et al (2010) DHPR α1S subunit controls skeletal muscle mass and morphogenesis. EMBO J 29:643–654. https://doi.org/10.1038/emboj.2009.366

35. Dirksen RT (2002) Bi-directional coupling between dihydropyridine receptors and ryanodine receptors. Front Biosci 7:d659–d670

36. Nakai J, Dirksen RT, Nguyen HT, Pessah IN, Beam KG, Allen PD (1996) Enhanced dihydropyridine receptor channel activity in the presence of ryanodine receptor. Nature 380:72–75. https://doi.org/10.1038/380072a0

37. Block BA, Imagawa T, Campbell KP, Franzini-Armstrong C (1988) Structural evidence for direct interaction between the molecular components of the transverse tubule/sarcoplasmic reticulum junction in skeletal muscle. J Cell Biol 107:2587–2600. https://doi.org/10.1083/jcb.107.6.2587

38. Paulin D, Li Z (2004) Desmin: a major intermediate filament protein essential for the structural integrity and function of muscle. Exp Cell Res 301:1–7. https://doi.org/10.1016/j.yexcr.2004.08.004

39. Franck A, Lainé J, Moulay G, Lemerle E, Trichet M, Gentil C et al (2019) Clathrin plaques and associated actin anchor intermediate filaments in skeletal muscle. Mol Biol Cell 30:579–590. https://doi.org/10.1091/mbc.E18-11-0718

40. Goldfarb LG, Dalakas MC (2009) Tragedy in a heartbeat: malfunctioning desmin causes skeletal and cardiac muscle disease. J Clin Invest 119:1806–1813. https://doi.org/10.1172/JCI38027

41. Goyal U, Blackstone C (2013) Untangling the web: mechanisms underlying ER network formation. Biochim Biophys Acta 1833:2492–2498. https://doi.org/10.1016/j.bbamcr.2013.04.009

42. Michelucci A, Boncompagni S, Pietrangelo L, García-Castañeda M, Takano T, Malik S et al (2019) Transverse tubule remodeling enhances Orai1-dependent Ca^{2+} entry in skeletal muscle. Elife 8:e47576. https://doi.org/10.7554/eLife.47576

43. Boncompagni S, Michelucci A, Pietrangelo L, Dirksen RT, Protasi F (2017) Exercise-dependent formation of new junctions that promote STIM1-Orai1 assembly in skeletal muscle. Sci Rep 7:14286. https://doi.org/10.1038/s41598-017-14134-0

44. Masiero E, Agatea L, Mammucari C, Blaauw B, Loro E, Komatsu M et al (2009) Autophagy is required to maintain muscle mass. Cell Metab 10:507–515. https://doi.org/10.1016/j.cmet.2009.10.008

Publisher's Note